ARTICLE

Check for updates

Organic photostimulated luminescence associated with persistent spin-correlated radical pairs

Manabu Sakurai[1], Ryota Kabe[2,3 ✉], Masaaki Fuki[4], Zesen Lin[2,3], Kazuya Jinnai[3,5], Yasuhiro Kobori [1,4], Chihaya Adachi [3,5,6] & Takashi Tachikawa [1,4 ✉]

Photostimulated luminescence allows energy or data to be stored and released using electromagnetic waves as both the input and output, and has attracted considerable interest in the fields of biomedical and information technologies. However, this phenomenon is mostly limited to solid inorganic materials. Here, we report photostimulated luminescence from purely organic blend films, composed of electron donor, acceptor, and trap/emitter molecules. Charges in the films are accumulated as radical ions by ultraviolet light irradiation and then extracted by near-infrared light irradiation. Even after storage in the dark for one week they produce visible light with good repeatability, color tunability, and are responsive to weak external magnetic fields. These findings might broadly impact existing applications and provide new prospects for innovative flexible devices.

[1] Department of Chemistry, Graduate School of Science, Kobe University, Kobe, Japan. [2] Organic Optoelectronics Unit, Okinawa Institute of Science and Technology Graduate University, Okinawa, Japan. [3] JST, ERATO ADACHI Molecular Exciton Engineering Project, Kyushu University, Fukuoka, Japan. [4] Molecular Photoscience Research Center, Kobe University, Kobe, Japan. [5] Center for Organic Photonics and Electronics Research (OPERA), Kyushu University, Fukuoka, Japan. [6] International Institute for Carbon Neutral Energy Research (WPI-I2CNER), Kyushu University, Fukuoka, Japan. ✉email: ryota. kabe@oist.jp; tachikawa@port.kobe-u.ac.jp

Organic semiconductors are promising materials for future technologies, such as flexible optoelectronic devices, high-density data storage, and biophotonics, owing to their structural diversity, mechanical elasticity, low cost, and facile processing[1–4]. Optical and electronic properties of these materials can be tailored through molecular design to yield efficient light emission or electric power conversion with tunable bandgap energies.

Recently, organic long persistent luminescence (LPL) systems producing a glow-in-the-dark effect have been demonstrated by retaining long-lived charge-separated states (CSSs) over periods of up to an hour at room temperature in blend films consisting of two or more organic compounds[5,6]. These systems are free of rare metals and can be fabricated via simple melt-casting at relatively low temperatures or solution processing at room temperature. Since then, a variety of organic LPL materials have been developed by combining different electron donor/acceptor pairs[7–10].

Meanwhile, conventional rare metal-based LPL systems are known to exhibit intense photostimulated luminescence (PSL), in which excess charges are accumulated at defects or dopant sites during pre-illumination (e.g., X-ray) and then be released by second illumination (e.g., visible light) to emit photons for a variety of applications (e.g., BaFBr:Eu^{2+} imaging plate)[11–14]. In addition, the long-lived charges in LPL materials are a promising candidate for coherent spin manipulation logic devices[15,16] and magnetic luminescence manipulation[17]. However, these applications are limited by prompt spin relaxation, usually in the nanosecond range, due to spin–orbit coupling in inorganic materials containing heavy atoms. The development of organic PSL materials would thus open up new fields of flexible optoelectronic devices and biomedical tools.

In this paper, we demonstrate purely organic PSL over a wide range of colors utilizing ultraviolet (UV) and near-infrared (NIR) light for multiple write-in and read-out cycles, respectively, by adding a molecule with dual roles as an electron trap and light emitter to the organic LPL systems. The slower spin relaxation in the absence of heavy atoms allowed manipulation of the LPL/PSL processes by weak external magnetic fields.

Results
Organic PSL systems. As a model system, we first explore a ternary blend film of electron donor (4,4′,4″-tris[(3-methylphenyl)phenylamino]triphenylamine; m-MTDATA) (1 mol%), electron acceptor (2,8-bis(diphenylphosphoryl)dibenzo[b,d]thiophene; PPT), and electron trap/emitter (5,6,11,12-tetraphenyltetracene; Rb) (1 mol%, unless otherwise noted) (Fig. 1a).

Excitation of the film with UV light induces the formation of CSSs between m-MTDATA and PPT, resulting in a green-emitting charge transfer (CT) excited state or exciplex (Fig. 1b)[18]. The excitation energy of the CT excited state is transferred to Rb via Förster resonance energy transfer, resulting in persistent orange emission (see Supplementary Note 1 and Supplementary Figures 1 and 2)[6]. At the same time, a portion of the electrons are captured by neutral Rb molecules, which have lowest unoccupied molecular orbitals (LUMOs) that are ~0.8 eV lower than that of PPT, to form the long-lived radical anions of Rb (Rb$^{•-}$) (Fig. 1c). Since Rb$^{•-}$ possesses strong absorption bands in the NIR region, NIR excitation can induce electron transfer from doublet excited Rb$^{•-}$ to neighboring PPT molecules, thereby producing mobile electrons in the PPT film for the generation of singlet excited state of Rb (^{1}Rb*).

Properties of organic PSL. Optical write-in and read-out processes based on organic PSL are schematically illustrated in Fig. 2a. First, an organic film is exposed to UV light for ~1 min to write in information. The irradiated film is kept in the dark for a defined time and then exposed to NIR light for reading out the stored information as visible PSL. Figure 2b displays a photograph of the m-MTDATA/PPT/Rb film prepared by reported procedures in an argon-filled glove box[6]. After stopping UV irradiation, orange LPL was clearly seen from the film, except for from the masked region, and gradually weakened over time. Surprisingly, NIR light irradiation of the film dramatically enhanced this orange emission to the point of being visible to the naked eye after keeping the film in the dark at room temperature for one day after stopping UV irradiation and with a commercial digital camera 1 week after UV irradiation (Fig. 2c). The irradiated triangular area seemed to have been retained to ensure long-term storage ability.

Luminescence properties of the uniform films were selectively examined by using an inverted fluorescence microscope (Supplementary Figure 3). As shown in Fig. 2d and Supplementary Figure 4, the LPL intensity suddenly increased more than 15 times upon NIR irradiation (see the arrow) without apparent changes in the spectral shape (Supplementary Figure 5), while no emission enhancement was observed without UV pre-irradiation. This observation is indicative of PSL, which could be repeated for ten write-in/read-out cycles for the same area with an ~10% loss in initial intensity (see Supplementary Note 1 and Supplementary Figure 6).

To confirm the existence of Rb$^{•-}$, we measured optical absorption spectra for the m-MTDATA/PPT/Rb films before and after UV irradiation, and then derived differential spectra. The characteristic absorption bands of Rb$^{•-}$ were observed at ~800 and 1000 nm[19] only for the film containing Rb (Fig. 2e and Supplementary Figure 7), while both films exhibited a broad band from 900 to 1400 nm, which is analogous to the absorption spectrum of m-MTDATA radical cations (m-MTDATA$^{•+}$)[20]. The absorption decayed slowly over time after stopping UV irradiation, indicating a gradual depletion of radical species accumulated in the film (see Supplementary Notes 2 and 3 and Supplementary Figures 8 and 9). The involvement of Rb$^{•-}$ was further supported by electron spin resonance (ESR) spectral measurements (see Supplementary Note 4 and Supplementary Figure 10).

To verify the origin of PSL, an action spectrum, where intensity changes upon NIR stimulation are plotted as a function of excitation wavelength, was measured (Supplementary Figure 11). The obtained spectral shape roughly matches the absorption spectrum of Rb$^{•-}$, thus suggesting the importance of spectral matching between stimulation light and electronic absorption of radical anions of trap/emitter molecules. A negligible enhancement seen for the film without trap/emitter molecules is possibly due to a small extinction coefficient (ε) of PPT$^{•-}$ (Fig. 2e), as compared with Rb$^{•-}$ ($\varepsilon \approx 2 \times 10^4\,\mathrm{M^{-1}\,cm^{-1}}$ at ~800 nm)[19].

Color tenability. The proposed scheme is applicable for color tuning with different trap/emitter molecules (2,5,8,11-tetra-tert-butylperylene (TBPe), 9,10-bis[N,N-di-(p-tolyl)-amino]anthracene (TTPA), 2,8-di-tert-butyl-5,11-bis(4-tert-butylphenyl)-6,12-diphenyltetracene (TBRb), and 4-(dicyanomethylene)-2-methyl-6-julolidyl-9-enyl-4H-pyran (DCM2)) whose LUMO levels are lower than that of PPT (−2.2 eV). All the samples exhibited detectable PSL with different colors and spectra similar to their LPL without NIR irradiation (Fig. 3 and Supplementary Figure 5). Compared with TBRb and DCM2, relatively weak NIR responses were observed for TBPe and TTPA. Since these molecules have LUMO energies lower than the others, we can exclude the possibility that the PSL simply originates from the thermal release of electrons from trap sites by NIR irradiation. In fact, significant
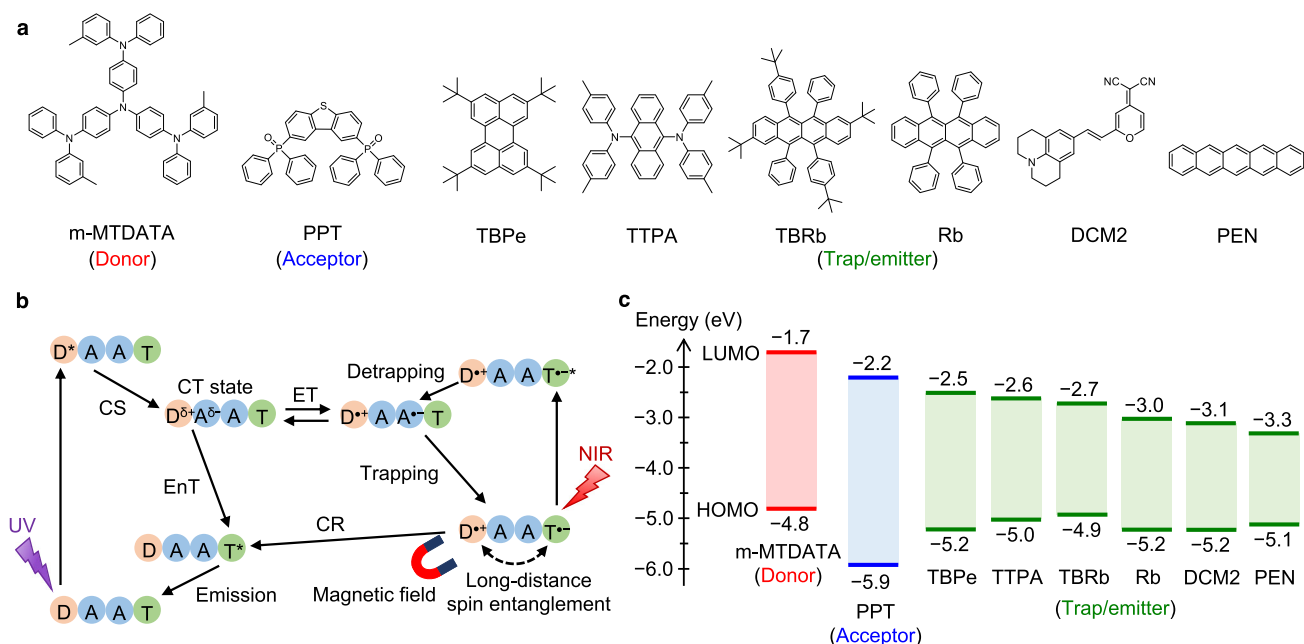
Fig. 1 Schematic illustration of organic PSL systems. a Molecular structures of m-MTDATA, PPT, and trap/emitter molecules. **b** Proposed reaction scheme of organic PSL. During UV excitation, an electron is transferred from the excited state of donor (D) to acceptor (A) to form the CT excited state or exciplex ($D^{\delta+}A^{\delta-}$). The electrons in the film diffuse between A molecules and are partly captured by trap/emitter (T) molecules, forming their radical anions ($T^{\bullet-}$). The excited state of $T^{\bullet-}$ ($T^{\bullet-*}$) formed by NIR stimulation causes electron transfer to A. The excited state of T (T^*) is then formed via FRET from the regenerated CT state or superexchange charge recombination, resulting in visible PSL. The luminescence from T^* is also modulated by external magnetic fields through long-distance spin entanglement between singlet and triplet states of the $D^{\bullet+}\cdots T^{\bullet-}$ pair. EnT energy transfer, ET electron transfer, CS charge separation, and CR charge recombination. **c** Highest occupied molecular orbital (HOMO) and LUMO levels of m-MTDATA, PPT, and trap/emitter molecules.

PSL was observed for the m-MTDATA/PPT/Rb film even at 77 K (Supplementary Figure 12). In the case of TBPe, the weak PSL may be due to inefficient excitation of radical anions since TBPe$^{\bullet-}$ has very weak absorption bands in the NIR region[21]. These results also suggest that trapping of electrons at depths deeper than 0.5 eV from the LUMO level of PPT could be necessary for intense PSL.

Magnetic field effects. Besides the NIR stimulation, the spin state of trapped charges could be controlled by magnetic fields. Here, we demonstrate magnetic field effects (MFEs) on LPL/PSL by applying external magnetic fields (B) with an electromagnet to the sample under the inverted fluorescence microscope[22]. Interestingly, significant decreases of emission intensity (i.e., negative MFEs) were observed for LPL/PSL (Fig. 4a and Supplementary Figure 13a, b), while no MFE was seen for the film without Rb (Supplementary Figure 13c), implying a crucial role of trap/emitter molecules. The MFEs in the LPL process can be expressed as

$$\chi_{\mathrm{LPL}}(B) = \frac{\mathrm{LPL}(B,t) - \mathrm{LPL}(0,t)}{\mathrm{LPL}(0,t)} \qquad (1)$$

where LPL(B,t) and LPL($0,t$) represent the LPL intensity at time t in the presence and absence of magnetic field, respectively. The $\chi_{\mathrm{LPL}}(B)$ values were plotted as a function of B and were then fitted by the Lorentzian function (inset of Fig. 4a). The absolute values of saturated $\chi_{\mathrm{LPL}}(B)$ increased with increasing Rb concentration, while the $B_{1/2}$ values (defined as the magnetic field at which the change in emission intensity reaches half of its saturation value) remained constant (see Supplementary Note 5 and Supplementary Figure 13d, e). Meanwhile, an increase of emission intensity (i.e., positive MFEs) was observed for fluorescence from the films both with and without Rb under UV irradiation (see Supplementary Note 6 and Supplementary Figure 14).

Discussion

Rb molecules are known to exhibit upconversion (UC) photoluminescence through triplet–triplet annihilation (TTA) of excited triplet states in both the solution and solid state[23–25]. To investigate the involvement of TTA-UC in the mechanism of PSL, we measured the luminescence of the ternary blend film containing pentacene (PEN) (1 mol%), in which TTA-UC is energetically impossible[26]. Considering the LUMO level (ca. −3.3 eV) of PEN[27], photogenerated electrons in the film can be captured by neutral PEN molecules (Fig. 1c). In addition, PEN$^{\bullet-}$ has an absorption band in the NIR region (700−900 nm) for stimulation[27]. As demonstrated in Supplementary Figure 15, a strong PSL was confirmed by doping PEN instead of Rb, supporting our newly proposed mechanism and its versatile applicability (see Supplementary Discussion 1 for a discussion of the mechanism of PSL).

In organic LPL materials, a number of CSSs are stored in the film under and after pre-excitation (Supplementary Figures 8 and 9). As shown in Fig. 4b, the spin distribution progresses to a singlet–triplet equilibrium in a statistical ratio of 1:3 when the spin mixing effectively occurs within the lifetime of spin-correlated CSSs. The luminescent species (singlet CT (^{1}CT) state or singlet excited state of Rb (^{1}Rb*)) were formed from singlet CSSs (^{1}CSSs) via slow detrapping process with the rate (k_{detr}) of 10^{-2}–10^0 s^{-1} (see the mechanism of MFEs in the Supplementary information)[28]. The NIR stimulation of ^{1}CSSs increases the proportion of luminescent species by accelerating the detrapping process (see the PSL process in Fig. 4c). In the presence of B of ~10 mT, the Zeeman splitting suppresses the population flow from ^{3}CSS to ^{1}CSS by reducing the rate of spin mixing between ^{3}CSS$_\pm$ and ^{1}CSS ($k_0 \approx 10^8$ s^{-1}, which was estimated from $B_{1/2}$) to the spin relaxation rate ($k_{\mathrm{rel}} = 10^3$–10^6 s^{-1})[16], and thus decreases the LPL/PSL intensity (see the MFE process in Fig. 4c). For the appearance of MFEs, modified spin
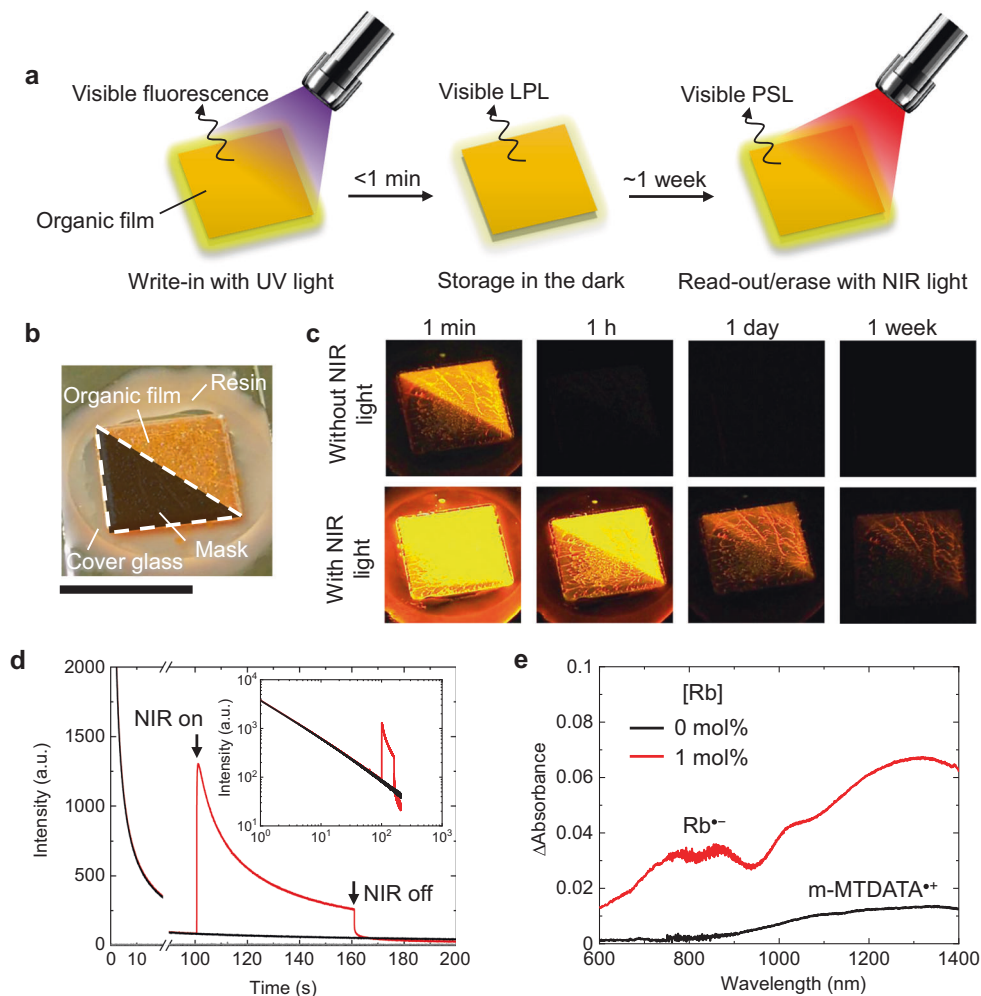
Fig. 2 Organic PSL from the m-MTDATA/PPT/Rb blend films. a Write-in and read-out processes. **b** Photograph of the m-MTDATA/PPT/Rb film. A part of the sample was masked during UV light irradiation. The scale bar is 10 mm. **c** Photographs of the samples without and with 800-nm light irradiation after stopping 365-nm light irradiation. **d** Emission decay profiles obtained for the m-MTDATA/PPT/Rb film with and without 800-nm light irradiation (red and black lines, respectively). The decay profile observed without UV pre-irradiation is also shown (gray line). The emission intensity was integrated over the wavelength range of 500−700 nm (Supplementary Figure 5d). The inset shows the logarithmic plots of the decay profiles. **e** Differential absorption spectra obtained for the m-MTDATA/PPT/Rb (0, 1 mol%) films before and after 365-nm light irradiation.

distribution through spin entanglement should maintain within the relaxation time (i.e., $k_{detr} \geq k_{rel}$). One possible reaction pathway is that long-distance ^{1}CSSs in the film containing Rb molecules as deep traps recombine to generate ^{1}Rb* via superexchange-mediated hole transfer[29] with rates faster than the spin relaxation (see Supplementary Discussion 2 for a discussion of the mechanism of MFEs and Supplementary Figure 16), as opposed to a recent mobile long-lived carrier dynamics in ZnS nanocrystal that exhibited no MFE[30]. Meanwhile, the undoped systems may not fit the above criteria for LPL, possibly due to smaller k_0 at shorter charge separation distances[31] and/or higher k_{rel} for PPT$^{•-}$ possessing heavier sulfur and phosphorus atoms[32].

The responsiveness to magnetic fields ($B_{1/2} \approx 3$ mT) observed for the present systems is distinguishable from that ($B_{1/2} > 100$ mT) reported for the Rb-based system exhibiting singlet fission[33] and makes them attractive for applications. Combined with write-in and read-out characteristics of PSL, manipulation of long-lived spin states in organic materials by weak magnetic fields will energize researchers in various fields such as molecular spintronics, which is a promising next-generation technology[34–36].

Methods

Materials. m-MTDATA (purity 99.4%, high-performance liquid chromatography (HPLC)) and Rb (purity 99.9%, gas chromatography) were obtained from Sigma-Aldrich (USA) and PPT (purity 99.9%, HPLC) was synthesized according to the literature[37]. These materials were purified by sublimation. TBPe (sublimed, purity >99%, HPLC), TTPA (sublimed, purity >99%, HPLC), TBRb (sublimed, purity >99%, HPLC), and DCM2 (purity >99%, HPLC) were obtained from Luminescence Technology Corp. (Taiwan) and used without purification. PEN (sublimed, purity 99.999%) was obtained from Tokyo Chemical Industry Co., Ltd (Japan) and used without purification. Purities of m-MTDATA and PPT were analyzed by HPLC (Waters, Alliance e2695) by using InertSustain C18 column (GL Science) (Supplementary Figure 17), and purities of other compounds are based on the specification of the suppliers. The predicted density of PPT using Advanced Chemistry Development (ACD/Labs) software was taken from SciFinder for calculation of molecular distance.

Sample fabrication. The ternary blend films were prepared by reported procedures[6]. Briefly, m-MTDATA (1 mol%), PPT (98 mol%), and trap/emitter molecules (1 mol%, unless otherwise noted) were dissolved in dichloromethane. Then, the solvent was removed under reduced pressure in the dark. The mixture was dried using three cycles of the freeze-pump method. In an argon-filled glove box, the dried mixture was placed on a glass plate and heated up to 250 °C for 10 s. After melting, the substrate was rapidly cooled down to room temperature and encapsulated using a cover glass and UV-cured epoxy resin (Fig. 2b). For low-temperature experiments, a quartz glass tube containing a mixture of PPT (98 mol %), m-MTDATA (1 mol%), and Rb (1 mol%) was evacuated under vacuum at
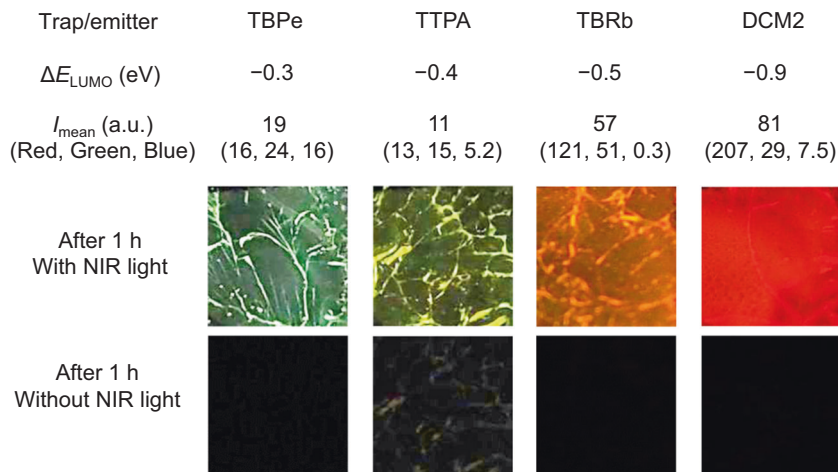
Trap/emitter	TBPe	TTPA	TBRb	DCM2
ΔE_{LUMO} (eV)	−0.3	−0.4	−0.5	−0.9
I_{mean} (a.u.) (Red, Green, Blue)	19 (16, 24, 16)	11 (13, 15, 5.2)	57 (121, 51, 0.3)	81 (207, 29, 7.5)
After 1 h With NIR light				
After 1 h Without NIR light				

Fig. 3 Color tuning of PSL with different trap/emitter molecules. Molecular structures of trap/emitter molecules and corresponding photographs of the blend films containing different trap/emitter molecules (1 mol%) with and without 800-nm light irradiation after stopping 365-nm light irradiation. The actual size of the films in the images is 5 mm × 5 mm. The difference of LUMO energy (ΔE_{LUMO}) was calculated from E_{LUMO} (trap/emitter) − E_{LUMO} (PPT) based on the reduction potentials of the materials (Fig. 1c). The mean intensity (I_{mean}) of PSL was calculated from the red, green, and blue components of the color image taken by a digital camera. The exposure time was 10 s. The brightness and contrast of images are different for each sample.
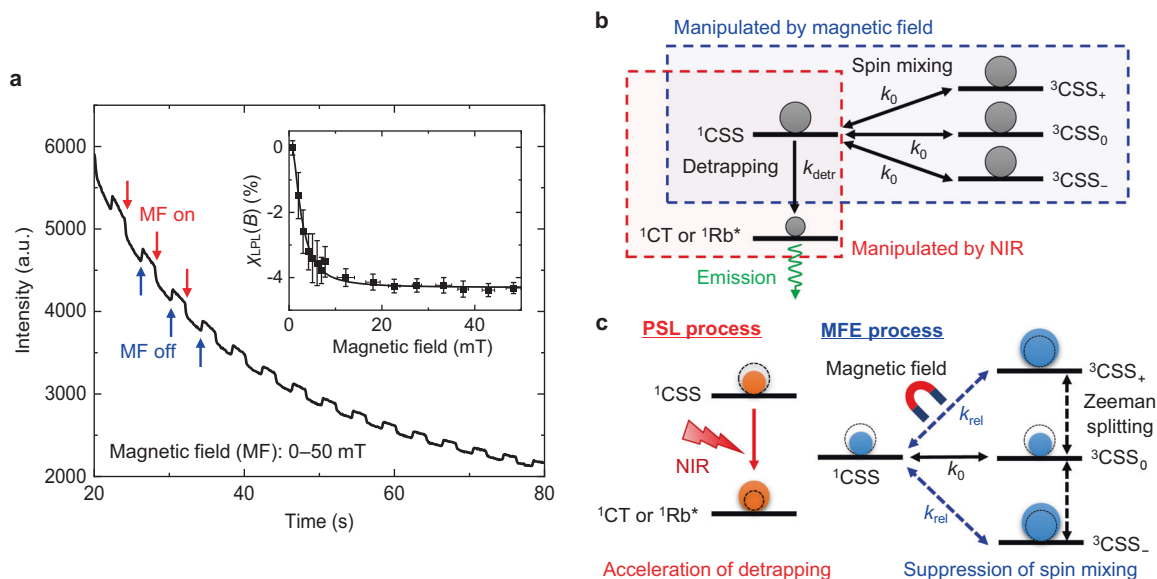

Fig. 4 Magnetic field effects. a The response of LPL intensity to the external magnetic fields observed for the m-MTDATA/PPT/Rb film. The inset shows the plots of $\chi_{LPL}(B)$ as a function of the external magnetic field (B). The solid line shows the least-squares fit of data to the Lorentzian function. **b** A schematic illustration of spin mixing between singlet and triplet CSSs ($^{1/3}$CSSs) and detrapping. $k_{detr} = 10^{-2}$–10^0 s^{-1}. $k_0 \approx 10^8$ s^{-1}. **c** A proposed model for NIR and magnetic field-induced population changes (circles in dotted lines) of luminescent species and $^{1/3}$CSSs. $k_{rel} = 10^3$–10^6 s^{-1}.

room temperature and then heated up to 250 °C to melt the mixture. After cooling down to room temperature, the sample tube was inserted into a transparent glass Dewar vessel. The vessel was filled with liquid nitrogen for emission measurements at 77 K.

Characterizations. To observe PSL, the sample was excited by monochromatic NIR light (e.g., 800 nm, 12 mW cm^{-2} at the sample) emitted from a Xe lamp (Asahi Spectra, MAX-303) with a bandpass filter, after stopping UV light irradiation (365 nm, 35 mW cm^{-2} at the sample) using an LED light source (Thorlabs, M365LP1). Before repeated experiments, the sample was exposed to intense NIR light (750–1050 nm) from the Xe lamp for 10 min to remove as many long-lived trapped electrons as possible. The optical absorption spectra were obtained using UV–vis–NIR spectrophotometer (JASCO, V-770). The NIR-induced changes of absorption spectra were obtained using the SEC2020 spectrometer system (BAS) and 785 nm laser (Thorlabs, LDM785). The cyclic voltammetry was carried out using an electrochemical analyzer (BAS, Model 610E). The measurements were performed in dried and oxygen-free dichloromethane (CH$_2$Cl$_2$) or N,N-

dimethylformamide (DMF) using 0.1 M tetrabutylammonium hexafluorophosphate (TBAPF$_6$) as a supporting electrolyte. A platinum fiber was used as a working electrode, glassy carbon as a counter electrode, and Ag/Ag$^+$ as a reference electrode. Redox potentials were referenced against ferrocene/ferrocenium (Fc/Fc$^+$). The HOMO level of m-MTDATA and LUMO levels of PPT and trap/emitter molecules (excepting PEN[27]) were calculated according to the equations of E_{HOMO} or $_{LUMO} = -E_{redox}$ (vs. Fc/Fc+) -4.8 eV[38]. The energy gaps between HOMO and LUMO levels were calculated from the onsets of the absorption spectra observed for solution samples. The absorption spectra of radical anion or radical cation of the materials were obtained by UV–vis–NIR spectrophotometer (Shimadzu, UV-3600 Plus). Samples in dried and oxygen-free CH$_2$Cl$_2$ or DMF with 0.1 M TBAPF$_6$ were oxidized or reduced by the platinum mesh electrode through the use of an electrochemical analyzer (BAS, Model 610E).

Fluorescence microscopy measurements. The fluorescence microscopy measurements were performed on an inverted fluorescence microscope (Nikon, Ti-E). A 365-nm LED (Thorlabs, M365LP1; 0.85 W cm^{-2} at the sample) was used to

excite the sample through an objective lens (CFI Plan Apo λ 100 × H, Nikon; NA (numerical aperture) = 1.45). A 810-nm LED light source (Thorlabs, M810L3; 810 nm, 12 mW cm^{-2} at the sample) was used for NIR stimulation. A Xe lamp (Asahi Spectra, MAX-303) and bandpass filters were used for NIR excitation with the same numbers of emitted photons to obtain the action spectrum. The NIR light was irradiated from above the sample. The emission from the sample was collected by the same objective lens, after which it was magnified by a 1.5× built-in magnification changer. It subsequently passed through a dichroic mirror (Semrock, FF697-SDI01 or Di02-R405) and a short-pass filter (Semrock, FF02-694/SP-25) or a long-pass filter (Semrock, BLP01-405R) to remove the undesired scattered light. The emission images were recorded with an electron-multiplying charge-coupled device camera (Roper Scientific, Evolve 512) using Micro-Manager (https://www.micro-manager.org/). The intensity profiles were obtained by subtracting the dark counts from the raw data. For the spectroscopy, only the emission that passed through a long-pass filter (Semrock, BLP01-405R) and a slit entered the imaging spectrograph (SOL instruments, MS3504i) equipped with a CCD camera (Andor, DU416A-LDC-DD). Magnetic fields were applied using a custom-made electro-magnet and calibrated with a gauss meter. All experimental data were obtained at room temperature unless otherwise noted.

Data availability
The data associated with the reported findings are available in the manuscript or the Supplementary information. Other related data are available from the corresponding authors upon request.

References

1. Friend, R. H. et al. Electroluminescence in conjugated polymers. *Nature* **397**, 121–128 (1999).
2. Lu, L. et al. Recent advances in bulk heterojunction polymer solar cells. *Chem. Rev.* **115**, 12666–12731 (2015).
3. Rivnay, J. et al. Organic electrochemical transistors. *Nat. Rev. Mater.* **3**, 17086 (2018).
4. Li, J. & Pu, K. Development of organic semiconducting materials for deep-tissue optical imaging, phototherapy and photoactivation. *Chem. Soc. Rev.* **48**, 38–71 (2019).
5. Kabe, R. & Adachi, C. Organic long persistent luminescence. *Nature* **550**, 384–387 (2017).
6. Jinnai, K., Kabe, R. & Adachi, C. Wide-range tuning and enhancement of organic long-persistent luminescence using emitter dopants. *Adv. Mater.* **30**, 1800365 (2018).
7. Lin, Z., Kabe, R., Nishimura, N., Jinnai, K. & Adachi, C. Organic long-persistent luminescence from a flexible and transparent doped polymer. *Adv. Mater.* **30**, 1803713 (2018).
8. Lin, Z., Kabe, R., Wang, K. & Adachi, C. Influence of energy gap between charge-transfer and locally excited states on organic long persistence luminescence. *Nat. Commun.* **11**, 191 (2020).
9. Nishimura, N., Lin, Z., Jinnai, K., Kabe, R. & Adachi, C. Many exciplex systems exhibit organic long-persistent luminescence. *Adv. Funct. Mater.* **30**, 2000795 (2020).
10. Alam, P. et al. Two are better than one: a design principle for ultralong-persistent luminescence of pure organics. *Adv. Mater.* **32**, 2001026 (2020).
11. Xu, J. & Tanabe, S. Persistent luminescence instead of phosphorescence: history, mechanism, and perspective. *J. Lumin.* **205**, 581–620 (2019).
12. Lakshmanan, A. R. Radiation induced defects and photostimulated luminescence process in BaFBr: Eu^{2+}. *Phys. Stat. Sol.* **153**, 3–27 (1996).
13. Rodríguez Burbano, D. C., Rodríguez, E. M., Dorenbos, P., Bettinelli, M. & Capobianco, J. A. The near-IR photo-stimulated luminescence of CaS:Eu^{2+}/Dy^{3+} nanophosphors. *J. Mater. Chem. C* **2**, 228–231 (2014).
14. Zhuang, Y., Katayama, Y., Ueda, J. & Tanabe, S. A brief review on red to near-infrared persistent luminescence in transition-metal-activated phosphors. *Opt. Mater.* **36**, 1907–1912 (2014).
15. Hanson, R. & Awschalom, D. D. Coherent manipulation of single spins in semiconductors. *Nature* **453**, 1043–1049 (2008).
16. Žutić, I., Fabian, J. & Das Sarma, S. Spintronics: fundamentals and applications. *Rev. Mod. Phys.* **76**, 323–410 (2004).
17. Pang, Z. et al. Manipulation of emission colors based on intrinsic and extrinsic magneto-electroluminescence from exciplex organic light-emitting diodes. *ACS Photonics* **4**, 1899–1905 (2017).
18. Jinnai, K., Nishimura, N., Kabe, R. & Adachi, C. Fabrication-method independence of organic long-persistent luminescence performance. *Chem. Lett.* **48**, 270–273 (2019).
19. Saeki, A., Seki, S., Takenobu, T., Iwasa, Y. & Tagawa, S. Mobility and dynamics of charge carriers in Rubrene single crystals studied by flash-photolysis microwave conductivity and optical spectroscopy. *Adv. Mater.* **20**, 920–923 (2008).
20. Matsushima, T. et al. Interfacial charge transfer and charge generation in organic electronic devices. *Org. Electron.* **12**, 520–528 (2011).
21. Karabunarliev, S., Gherghel, L., Koch, K.-H. & Baumgarten, M. Structure and optical absorption of oligorylenes upon doping. *Chem. Phys.* **189**, 53–65 (1994).
22. Sakurai, M., Kobori, Y. & Tachikawa, T. Structural dynamics of lipid bilayer membranes explored by magnetic field effect based fluorescence microscopy. *J. Phys. Chem. B* **123**, 10896–10902 (2019).
23. Islangulov, R. R., Kozlov, D. V. & Castellano, F. N. Low power upconversion using MLCT sensitizers. *Chem. Commun.* **5**, 3776–3778 (2005).
24. Liu, H. et al. Up-conversion luminescence of crystalline rubrene without any sensitizers. *Org. Electron.* **11**, 946–950 (2010).
25. Cruz, C. D., Choi, H. H., Podzorov, V., Chronister, E. L. & Bardeen, C. J. Photon upconversion in crystalline Rubrene: resonant enhancement by an interband state. *J. Phys. Chem. C* **122**, 17632–17642 (2018).
26. Wilson, M. W. B., Rao, A., Ehrler, B. & Friend, R. H. Singlet exciton fission in polycrystalline pentacene: from photophysics toward devices. *Acc. Chem. Res.* **46**, 1330–1338 (2013).
27. Enengl, S. et al. Spectroscopic characterization of charge carriers of the organic semiconductor quinacridone compared with pentacene during redox reactions. *J. Mater. Chem. C* **4**, 10265–10278 (2016).
28. Chen, R. On the calculation of activation energies and frequency factors from glow curves. *J. Appl. Phys.* **40**, 570–585 (1969).
29. Winkler, J. R. & Gray, H. B. Long-range electron tunneling. *J. Am. Chem. Soc.* **136**, 2930–2939 (2014).
30. Han, Y. et al. Fast T-type photochromism of colloidal Cu-doped ZnS nanocrystals. *J. Am. Chem. Soc.* **143**, 2239–2249 (2021).
31. Woodward, J. R. Radical pairs in solution. *Prog. React. Kinet. Mech.* **27**, 165–207 (2002).
32. Yu, Z. G. Spin-orbit coupling, spin relaxation, and spin diffusion in organic solids. *Phys. Rev. Lett.* **106**, 106602 (2011).
33. Nagata, R., Nakanotani, H., Potscavage, W. J. & Adachi, C. Exploiting singlet fission in organic light-emitting diodes. *Adv. Mater.* **30**, 1801484 (2018).
34. Wolf, S. A. Spintronics: a spin-based electronics vision for the future. *Science* **294**, 1488–1495 (2001).
35. Ratera, I. & Veciana, J. Playing with organic radicals as building blocks for functional molecular materials. *Chem. Soc. Rev.* **41**, 303–349 (2012).
36. Lupton, J. M., McCamey, D. R. & Boehme, C. Coherent spin manipulation in molecular semiconductors: getting a handle on organic spintronics. *ChemPhysChem* **11**, 3040–3058 (2010).
37. Fan, C. et al. Dibenzothiophene-based phosphine oxide host and electron-transporting materials for efficient blue thermally activated delayed fluorescence diodes through compatibility optimization. *Chem. Mater.* **27**, 5131–5140 (2015).
38. Pommerehne, J. et al. Efficient two layer leds on a polymer blend basis. *Adv. Mater.* **7**, 551–554 (1995).

Author contributions
R.K. and T.T. conceived the project. M.S., R.K., and T.T. prepared the samples and obtained the experimental data. M.F. and Y.K. performed ESR measurements and Gaussian calculations. Y.K. developed the theoretical description for MFEs. R.K., Z.L., and K.J. performed electrochemical and spectroelectrochemical measurements. C.A. partly guided the project. M.S., R.K., and T.T. wrote the manuscript with input from all authors.

Competing interests
The authors declare no competing interests.

Additional information

Supplementary information The online version contains supplementary material available at https://doi.org/10.1038/s43246-021-00178-3.

Correspondence and requests for materials should be addressed to R.K. or T.T.

Peer review information *Communications Materials* thanks the anonymous reviewers for their contribution to the peer review of this work. Primary handling editors: Jie Xu, John Plummer.

Reprints and permission information is available at http://www.nature.com/reprints

Publisher's note Springer Nature remains neutral with regard to jurisdictional claims in published maps and institutional affiliations.